

Research highlights

Cite this: *Lab Chip*, 2013, 13, 2179
DOI: 10.1039/c3lc90041j

Mark W. Tibbitt,^a Hojae Bae,^b Mehmet R. Dokmeci^{cd} and Ali Khademhosseini^{*cdef}

www.rsc.org/loc

Suffocating cancer: understanding cell–drug interactions during hypoxia

Oxygen deficiency, or hypoxia, often arises in the tumor microenvironment on account of an imbalance between oxygen consumption and supply.¹ Hypoxia is often related to increased tumor malignancy and resistance to treatment.¹ In many cases, the efficacy of an antitumor drug depends directly on the oxygen conditions in the tumor microenvironment.² Therefore, model systems to study the combinatorial effects of hypoxia and antitumor drugs on cancer cell fate could help improve cancer treatments. Current systems to study the effects of hypoxia on cells often rely on mixing or chemical deoxygenation that generates physiologic and uniform oxygen concentrations. Oxygen gradients are present in the tumor microenvironment and the ability to recapitulate such gradients *in vitro* is essential to elucidate the effects of hypoxia on cancer treatment.

To study the relationship between hypoxia and antitumor drugs in a robust manner, Wang *et al.* recently developed a microfluidic device that enables the generation of oxygen gradients in a series of microchambers that each possess a discrete concentration of a chemotherapy agent (Fig. 1).³ The chambers were functionalized to enable real-time reporting of the local oxygen concentration, and physiologic gradients were generated by tuning the media flow rate and chamber width. The unique design of the device defined the discrete concentrations of chemotherapy agents in each chamber. Cancer cells were then cultured within the microchambers to probe the combinatorial effect of oxygen gradients and chemotherapy drug concentrations on cancer cell fate.

^aThe David H. Koch Institute for Integrative Cancer Research, Massachusetts Institute of Technology, Cambridge, Massachusetts 02139, USA

^bCollege of Animal Bioscience and Technology, Department of Bioindustrial Technologies, Konkuk University, Hwayang-dong, Kwangjin-gu, Seoul 143-701, Republic of Korea

^cCenter for Biomedical Engineering, Department of Medicine, Brigham and Women's Hospital, Harvard Medical School, Cambridge, Massachusetts 02139, USA

^dHarvard-MIT Division of Health Sciences and Technology, Massachusetts Institute of Technology, Cambridge, Massachusetts 02139, USA

^eWyss Institute for Biologically Inspired Engineering, Harvard University, Boston, Massachusetts 02115, USA. E-mail: alik@rics.bwh.harvard.edu

^fWorld Premier International-Advanced Institute for Materials Research (WPI-AIMR), Tohoku University, Sendai 980-8577, Japan

The hypoxic microfluidic device was fabricated in polydimethylsiloxane (PDMS) with two inlets that fed into a circular ring with four evenly spaced serpentine channels that led to a second concentric ring with eight evenly spaced serpentine channels. The second layer of serpentine channels was fed into a cell culture microchamber with an outlet (Fig. 1). The inlets introduced two disparate concentrations of the chemotherapeutic agent into the device, while the rings and serpentine channels facilitated mixing and splitting of the media to generate five discrete concentrations of the chemotherapeutic agents in the terminal microchambers. The media was initially treated with Na₂SO₃ (4 g L⁻¹) to chemically consume all of the soluble oxygen at the inlets. Na₂SO₃ was employed as it depletes oxygen rapidly and generates a biocompatible reaction product (Na₂SO₄). The researchers exploited the rapid diffusion of oxygen through PDMS to generate oxygen gradients across the width of the terminal microchambers. At cell-compatible flow rates (0.5–2 μl min⁻¹), the oxygen-depleted media flowed quickly through the narrow (300 μm) concentric circles and serpentine channels before significantly interacting with oxygen in the wide (900 μm) microchambers. Interestingly, the surface of the microchambers was coated with a thin film of PDMS containing an indicator of local oxygen concentration (platinum octaethylporphorin, Pt-OEP). In this manner, the oxygen gradient within the microchambers was monitored in real time.

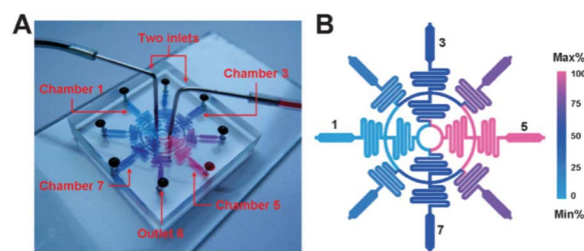


Fig. 1 A schematic illustration of the hypoxia chamber used for screening cell–drug interactions in a hypoxic environment. (a) The device was cast in PDMS with two inlets that fed a series of concentric rings and serpentine channels to generate controlled environments in the terminal microchambers. (b) The design enabled five discrete concentrations in the hypoxic microchambers so that a range of antitumor drugs could be screened in parallel. Figure reprinted with permission from the Royal Society of Chemistry from Wang *et al.*³

Highlight

The microchambers were then coated with the adhesive protein fibronectin ($50 \mu\text{g mL}^{-1}$) and cancer cells (A549 and HeLa cell lines) were cultured in the terminal microchambers. Oxygen-depleted media containing $100 \mu\text{M}$ of an antitumor drug, tirapazamine (TPZ) or bleomycin (BLM), was flowed through the device. Cell viability was quantified spatially across the device to determine how cells responded to the different drugs in a dynamic hypoxia microenvironment. The device revealed that TPZ efficacy increases in hypoxic environments, while BLM is more efficacious in normoxic environments.

This approach presents a viable method to better understand the combinatorial effects of hypoxia and antitumor drugs on cancer cell fate. Extending this system to a broad range of chemotherapeutics and cancer cell lines may instruct improved clinical therapies for cancer treatment. Furthermore, this approach is amenable to personalized medicine: culturing an individual's biopsied cancer cells within this device could elucidate the most effective treatment based on relative oxygen levels in the tumor.

Micromanufacturing antibodies

Since 1986, when the first monoclonal antibody received US FDA approval as a drug for human therapy (muromonab; Janssen-Cilag), the field of therapeutic antibodies has exploded.⁴ Prominent successes, *e.g.*, Herceptin (breast cancer; Genentech/Roche); Humira (autoimmune diseases; Trudexa/Abbott); Remicade (autoimmune diseases; Centocor/Merck); Rituxan/Mabthera (lymphoma, leukemia, and immune disorders; Genentech/Roche/Biogen Idec); and Avastin (angiogenesis inhibitor for cancer; Genentech), have propelled the industry to the top of the biological drug market.⁵ Monoclonal antibody therapy has focused on cancer and autoimmune diseases, but a range of other opportunities exist. However, many antibody treatments still remain costly, limiting their clinical use.

To mitigate the costs of antibody production, Garza-García *et al.* have recently developed a proof of concept continuous micro-bioreactor with significantly increased production of monoclonal antibodies.⁶ This micromanufacturing plant consisted of Chinese hamster ovary (CHO) cells cultured on the surface of a microfluidic device that continuously produces the antibody products under flow. The surface of the microreactor was micromachined to create pores $15 \mu\text{m}$ in diameter that facilitated cell attachment (Fig. 2a). Preliminary results with the continuous micro-bioreactor displayed a productivity three orders of magnitude higher than conventional batch reactors.

Most industrial processes produce monoclonal antibodies with suspended CHO cells in large volume stirred tanks. These batch or fed-batch reactors are expensive to operate, contributing to the high cost of most monoclonal antibody therapies. Increasing productivity is an attractive avenue to decrease costs and can be achieved with perfusion-based reactors.⁷ To adapt this concept to the microscale, Alvarez and

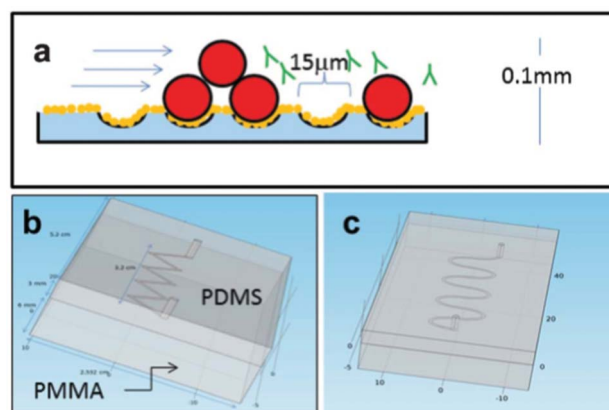


Fig. 2 A schematic illustration of the continuous micro-bioreactor for antibody production. (a) CHO cells (red) attached to microgrooves in the PMMA (blue) device. A FN (orange) coating improved cell attachment and continuous flow enabled the production and purification of monoclonal antibodies (green). (b) A jagged channel was employed as cells attached preferentially to the corners and the walls of the device. (c) Control, wavy channels exhibited lower cell attachment compared to the jagged channels. Figure reprinted with permission from the Royal Society of Chemistry from Garza-García *et al.*⁶

colleagues engineered a microfluidic device for CHO cell attachment, proliferation, and antibody production during continuous flow. A jagged microchannel ($400 \mu\text{m}$ wide with 90° corners) was cast in poly(methyl methacrylate) (PMMA) (Fig. 2b) and textured to facilitate CHO cell attachment. The jagged channels led to increased attachment as compared to smooth and wavy control channels (Fig. 2c) as cells preferentially attached to corners and walls, which are regions having lower flow velocities. A layer of fibronectin (FN) was deposited on the surface of the PMMA to improve cell attachment and increase the threshold for cell detachment ($>5 \mu\text{L min}^{-1}$).

A continuous feed ($5 \mu\text{L min}^{-1}$) of media entered the jagged microchannel ($V = 2.10 \mu\text{L}$) with an average residence time of ~ 25 s. To measure the reactor productivity, antibody concentrations in $100 \mu\text{L}$ samples at the outlet stream were measured. The antibody concentration in the FN-coated, jagged microreactors was found to vary between 1.66 and 2.04 mg L^{-1} measured over a period of two days. This implies a productivity of $4.75 \mu\text{g mL}^{-1} \text{ min}^{-1}$, which is three orders of magnitude higher than batch reactors. In comparison, fed-batch reactors produce antibodies at a rate of ($0.041 \mu\text{g mL}^{-1} \text{ min}^{-1}$), which is two orders of magnitude lower than continuous microreactors.

While continuous micro-bioreactors for antibody production are still in the early phase, this approach has promise for increased production and decreased cost of a range of monoclonal antibody therapeutics. Future studies should focus on the optimization of this process for a range of CHO cell lines and antibodies. Furthermore, a robust analysis of cost and materials for industrial-scale production of therapeutic antibodies *via* micromanufacturing is needed to translate this technology into the biotech sphere.

Blood diagnostics on a smart phone

Blood tests are one of the most common types of medical tests that provide valuable information for disease diagnosis. However, a typical blood test requires a rather large sample volume (at least 1 mL) and manual counting of blood cells is often subject to errors. Commercially available automated cell counters, such as flow cytometers are highly accurate, but consist of bulky and expensive equipment. Recent advances in personal mobile phone technology and massive investments in telecommunication infrastructure combined with an increased number of users have made the smart phone a ubiquitous platform for the development of various diagnostic applications. In this context, smart phone-based microscopy and its use in diagnostic applications has recently emerged as a research field in its own right.⁸ For example, a compact and cost-effective smart phone-based imaging cytometry platform, capable of rapid blood analysis with an accuracy comparable to commercially available flow cytometers, has been recently developed and demonstrated by Ozcan and co-workers.⁹

Zhu *et al.*⁹ developed a portable smart phone-based blood analyzer for rapid, but accurate, analysis of blood (white blood cells (WBC), red blood cells (RBC), and hemoglobin) with a simple preparation step that can potentially be used in point-of-care offices or in field environments where remote disease diagnosis is required. With minor modifications to a commercially available smart phone, a universal phone-based platform compatible with add-on units was developed (Fig. 3A). Three different add-on units (WBC imaging/counting, RBC imaging/counting, and hemoglobin density measurement) were built using inexpensive parts, such as plano-convex lenses and light emitting diodes (LEDs) (Fig. 3B–D). The add-on units can be attached onto the phone-base where their lenses are aligned with the lens of the phone for analysis.

For WBC analysis, fluorescently labeled WBCs in diluted blood were loaded into the cell-counting chamber (channel depth $\sim 100 \mu\text{m}$). Excitation ($\sim 470 \text{ nm}$) LEDs illuminated the sample symmetrically from two sides to provide a uniform excitation within the counting chamber. In addition, low-cost plastic filters were utilized to reject the scattered excitation light. The imaging of WBCs was enabled by the phone's built-in camera through a plano-convex lens placed between the blood sample and the camera lens. The RBC counting add-on unit was designed to image unlabelled RBCs in diluted blood samples using bright field illumination. Using the same base unit, the hemoglobin concentration in the blood sample was determined by measuring the light absorbance through a standard 1 cm cuvette containing lysed blood. Upon installation of the hemoglobin measurement add-on unit, the hemoglobin concentration was calculated using the recorded transmission light intensity acquired through the installed camera.

Images acquired using the above platform were then processed using a custom made mobile-phone application program to generate the results. The application enabled the user to choose a specific test type, followed by automated

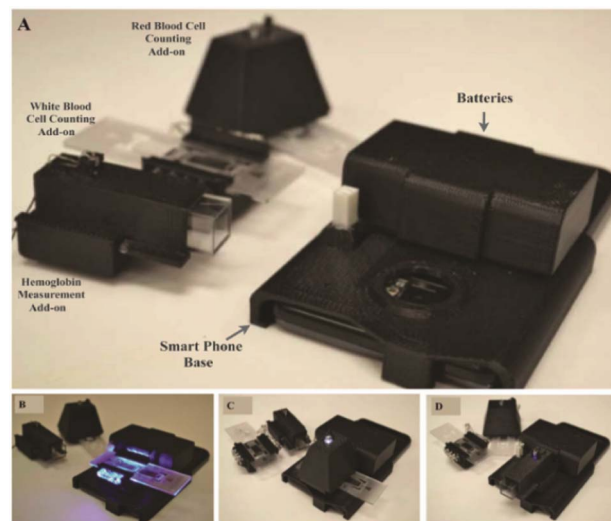


Fig. 3 A picture of the smart phone-based blood analysis platform. (A) The smart phone-based blood analysis platform consists of a battery, smart phone fixture for adapting three different add-on components, and three different add-on components (red blood cell counting, white blood cell counting, and hemoglobin measurements). (B and C) Images of the white and red blood cell counting add-ons. (D) An image of the hemoglobin measurement add-on. The add-on components can be attached to the smart phone analysis platform, such that their lenses are directly in contact with the existing camera lens on the phone, thereby forming a complete imaging system. Figure reprinted with permission from the Royal Society of Chemistry from Zhu *et al.*⁹

imaging of the sample of interest (corresponding to the add-on unit). The raw images were then processed using the following information: region of interest, pixel size, dilution factor, and channel height. After the calculation, the WBC and RBC results were reported as the number (#) of cells μL^{-1} and the hemoglobin concentration as g dL^{-1} . Furthermore, these results could be uploaded to a central database or server, to be further analyzed by healthcare professionals. To carry out the aforementioned calculations, an automated cell counting algorithm was developed for the application to reduce counting errors and shorten analysis time.

Finally, the performance of the developed hardware and software were verified through direct comparison with the results obtained from a commercially available hematology analyser (Sysmex KN21). The correlation coefficients acquired from the direct comparison of the WBC, RBC, and hemoglobin results were ~ 0.98 , ~ 0.98 , ~ 0.92 , respectively. Moreover, the absolute errors generated by the mobile-phone blood analyzer compared to the standard test results for the WBC, RBC, and hemoglobin were within 7%, 5%, and 5%, respectively.

This work demonstrates a cost-effective mobile phone-based blood analysis platform capable of rapidly yielding WBC and RBC numbers and hemoglobin density measurements that are comparable to a commercially available hematology analyzer. An appealing aspect of this platform is its compact nature that enables rapid analysis in the field. Furthermore, the measurements can either be stored on a phone or sent to a

healthcare professional for remote diagnostics, paving the way for numerous telemedicine applications.

References

- 1 P. Vaupel and L. Harrison, *Oncologist*, 2004, **9**, 4–9.
- 2 W. R. Wilson and M. P. Hay, *Nat. Rev. Cancer*, 2011, **11**, 393–410.
- 3 L. Wang, W. M. Liu, Y. L. Wang, J. C. Wang, Q. Tu, R. Liu and J. Y. Wang, *Lab Chip*, 2013, **13**, 695–705.
- 4 O. Leavy, *Nat. Rev. Immunol.*, 2010, **10**, 297–297.
- 5 A. Beck, T. Wurch, C. Bailly and N. Corvaia, *Nat. Rev. Immunol.*, 2010, **10**, 345–352.
- 6 L. D. Garza-García, L. M. Carrillo-Cocom, D. Araiz-Hernández, P. Soto-Vázquez, J. López-Meza, E. J. Tapia-Mejía, S. Camacho-León, E. García-López, C. A. Rodríguez-González and M. M. Alvarez, *Lab Chip*, 2013, **13**, 1243–1246.
- 7 V. Warikoo, R. Godawat, K. Brower, S. Jain, D. Cummings, E. Simons, T. Johnson, J. Walther, M. Yu, B. Wright, J. McLarty, K. P. Karey, C. Hwang, W. C. Zhou, F. Riske and K. Konstantinov, *Biotechnol. Bioeng.*, 2012, **109**, 3018–3029.
- 8 I. I. Bogoch, J. R. Andrews, B. Speich, J. Utzinger, S. M. Ame, S. M. Ali and J. Keiser, *Am. J. Trop. Med. Hyg.*, 2013, **88**, 626–629.
- 9 H. Zhu, I. Sencan, J. Wong, S. Dimitrov, D. Tseng, K. Nagashima and A. Ozcan, *Lab Chip*, 2013, **13**, 1282–1288.